Endocrine (2019) 63:639–650
https://doi.org/10.1007/s12020-018-1803-1

ORIGINAL ARTICLE

Overexpression of CAV3 facilitates bone formation via the Wnt signaling pathway in osteoporotic rats

Run-Bao Yang[1] · Feng-Fei Lin[2] · Jun Yang[1] · Bin Chen[2] · Ming-Hua Zhang[1] · Qiao-Ping Lu[1] · Bo Xiao[1] · Yan Liu[1] · Ke Zheng[2] · Yong-Rong Qiu[3]

Received: 6 June 2018 / Accepted: 20 October 2018 / Published online: 14 November 2018

Abstract

Purpose Osteoporosis is a condition characterized by decreased bone density and bone strength, commonly observed among older individuals. Caveolin-3 (CAV3) is a principal structural protein of the caveolae membrane domains, which has been reported to participate in cell signaling as well as the maintenance of cell structure. The aim of the current study was to investigate the effects involved with the silencing of CAV3 on bone formation among osteoporotic rat models via the Wnt signaling pathway.

Methods Osteoporosis was initially induced by means of ovariotomy among rat models in order to determine the expression of CAV3. Then, to confirm the specific function and mechanism of CAV3 from an osteoporosis perspective, the CAV3 expression vector was constructed and transfected into the osteoblasts of the osteoporotic rats. Afterward, the mRNA and protein expressions of CAV3, β-catenin, low-density lipoprotein receptor-related protein 5 (LRP5), T-cell factor (TCF), and Wnt3a in addition to cell proliferation and apoptosis were detected accordingly.

Results Positive expression of CAV3 exhibited diminished levels in the bone tissues of osteoporotic rats. The osteoblasts of the osteoporotic rats treated with overexpressed CAV3 displayed elevated mRNA and protein expression levels of β-catenin, LRP5, TCF, and Wnt3a. Increased cell proliferation and decreased cell apoptosis were also observed, while the osteoblasts of the osteoporotic rats treated with si-CAV3 exhibited an opposite result.

Conclusion Overexpressed CAV3 promotes bone formation and suppresses the osteoporosis progression via the activation of the Wnt signaling in rat models, suggesting CAV3 as a potential target biomarker in the treatment of osteoporosis.

Keywords Osteoporosis · CAV3 · Gene silencing · Wnt signaling pathway · Bone formation

Introduction

Osteoporosis is widely considered to be a significant public health stumbling block, often increasing an individual's susceptibility to fracture risk, particularly among the aged population, with the hip, humerus, and vertebrae particularly at risk [1]. Osteoporosis represents a disease resulting in decreased bone density and diminishing bone strength affecting bone support function [2]. Current literature has indicated that approximately 49 million people suffer from osteoporosis in a total of 9 industrialized regions with a higher female incidence than that of their male counterparts [3]. In China, various traditional agents with varying potencies have previously been employed throughout history tasked with preventing and treating osteoporosis, however, superior results have been observed when these agents are administered in combination with other drugs [4]. The progressive loss of bone mass inflicted by osteoporosis results in more fractures, highlighting the urgent need for novel treatments, approaches, and strategies [5]. Fresh perspectives from a genetic and molecular point of view are required in order to develop a more effective long-term

These authors are regarded as co-first authors: Run-Bao Yang, Feng-Fei Lin.

✉ Yong-Rong Qiu
qyr2299811@163.com

[1] Department of Orthopedics and Traumatology, Longyan First Hospital, Longyan 364000, P. R. China

[2] Department of Orthopedic Surgery, Fuzhou Second Hospital, Fuzhou 350007, P. R. China

[3] Department of Orthopaedics Surgery, Longyan First Hospital, Longyan 364000, P. R. China

model for chronic disorders such as osteoporosis on the basis of recent insights into bone cell functions [6].

Caveolin-3 (CAV3) is one of the six subsets of the protein caveolins (CAV-1, 2, 3), and also important for the formation of caveolae [7]. Caveolae are a subset of small (50–100 nm) plasma membrane invaginations that have been defined in the literature as "cave-like" structures, which are particularly abundant in most cell types participating in the cell response [8]. Existing literature has indicated that CAV2 is involved in the immune-response of bone marrow-derived macrophages [9]. Wnts are a type of Cys-rich protein encoded by 19 genes in humans, which in combination with an array of receptors act to induce different downstream pathways [10]. Research into the complex role of Wnt signaling has increased dramatically since its initial discovery, however a large degree of uncertainty remains regarding the function of Wnt's on different types of cancer [11]. For many years, Wnt signaling pathways have attached much importance in the recent research of bone biology owing to their critical role in the maintenance and development of bone mass and skeletal development [12]. Wnt6 has previously been verified as a novel target of caveolin-1 in gastric cancer cell [13], the complex crosstalk between caveolins and Wnt signaling still remains to be identified, especially in the field of osteoporosis. Based on our exploration of literature, the central objective of the current study was to explore the effects involved in the silencing of CAV3 on the formation of bone in osteoporotic rats via the Wnt signaling pathway.

Materials and methods

Study subjects

A total of 50 normal female SPF grade Wistar rats were recruited for the purposes of this study (age: 11 weeks old; mean weight: 247 ± 24.75 g; license number: SCXK Shandong Province 20170008; Experimental Animal Center of Zhongshan School of Medicine). The rats were permitted free access to feeding and water under conditions of 50–60% and humidity at 22–24 °C with a controlled day-night cycle of 12 h. All animal procedures during this study were performed in strict accordance with the local principles of management and use of experimental animals. Extensive efforts were made in order to minimize both the number of animals used as well as their respective suffering.

Establishment of osteoporotic rat models

After 1 week of adaptive feeding, the rats were randomly assigned into the osteoporosis group and sham group with 25 rats in each one. Ovariotomy was performed on the rats in order to establish osteoporosis rat models [14]. The model rats were anesthetized with 2% pentobarbital sodium at a dosage of 45 mg/kg under sterile conditions. After the bilateral ovariectomy was operated using the 1/3 position on either side of the abdomen, the abdomen, muscle, and skin were all successively sutured in two layers with complete hemostasis confirmed. Next, with the exception of the mesentery tissues the remaining structures were removed with the same weight, the rats in the sham group were operated on using the same incisions followed by the use of identical preoperative and postoperative procedures as the model establishment. Rats from both the groups had their respective stitches removed 1-week post operation, with stain smearing conducted over the next 7 days in order to ascertain as to whether cyclic variation occurred. 12 weeks later, the bone density of the entire body, femur and tibia was recorded. The rats in the osteoporosis and sham groups were fed under identical conditions.

Measurement of osteoblast and osteoclast

12 weeks post model establishment, 4 rats in each group were causally executed by means of cervical dislocation. The free bones at metaphysis distal to right-side femurs were cut into 5 mm thick sections and fixed with 10% formaldehyde for 4 h. After that, the bone tissue samples were immersed into the decalcifying fluid (5 ml of hydrochloric acid, 10 ml of formaldehyde and 85 ml of distilled water were reacted together) for 20 h till they became softened. Next, the samples were washed and filtered using running water, dehydrated, embedded, sectioned and stained with HE. The sections were obtained with each two made from one sample, followed by secondary dehydration and cleaning. Six fields (10 × 40) in each section were used to record the quantity of the osteoblasts and osteoclasts in the cancellous bone region of the metaphysis distal to the femur.

Measurement of serum alkaline phosphatase (ALP) and tartrate-resistant acid phosphatase (TRAP) levels

The rats were anesthetized with 200 g/L urethane at a dose of 10 ml/kg for exsanguination purposes from the arteriae coeliaea prior to execution. Next, the serum was centrifuged from drawn blood at 4000 rpm at room temperature for detecting the levels of ALP and TRAP. The ALP value was evaluated using an ALP detection kit and full-automatic biochemistry analyzer (Shanghai Manpu Biotechnology Co., Ltd., Shanghai, China) over a 2 h period, with detection conducted under strict accordance with the kit instructions. TRAP activity was measured under preconditions of 80 mmol/L sodium tartrate (pH 5.5) at 37 °C, and a unit of

enzyme activity subsequently classed with a yield of 1 μmoL of sodium tartrate to the quantity of nitrophenol.

Hematoxylin and eosin (HE) staining

At the 12th-week post model establishment, the bone tissue samples of 4 rats from each group that had been executed by cervical dislocation were extracted and fixed with 4% paraformaldehyde for 24 h. Following dehydration with 80%, 90%, 100% ethanol and n-butyl alcohol in a successive manner, the samples were immersed in 60 °C wax box, embedded and sectioned into 5 μm thick sections, spread out at 45 °C, picked up, roasted at 60 °C for 1 h and dewaxed using xylene. HE staining was then conducted after hydration. The sections were dewaxed, hydrated with gradient alcohol and stained with hematoxylin (Beijing Solarbio Science & Technology Co., Ltd., Beijing, China) for a 2 min period. After washing with water for 10 s, 1% hydrochloric acid-ethanol was used for color-separation purposes for 10 s. The sections were washed with distilled water for 1 min, stained with eosin for 1 min, and then distilled with water again for light washing for 10 s. Following alcohol dehydration and xylene cleaning, the sections were examined for morphological bone tissue morphological changes under an optical microscope (XP-330, Shanghai Bingyu Optical Instrument Co., Ltd., Shanghai, China) after sealing with neutral balsam.

Immunocytochemistry

A total of 6 rat bone tissue samples were extracted, fixed with formaldehyde, embedded with paraffin, made into 4 μm serial sections. The sections were baked in a 60 °C incubator for 1 h, dewaxed by xylene, dehydrated with gradient alcohol, then immersed in 3% H_2O_2 for 10 min and washed with distilled water. Antigen repair under high-pressure conditions was used for 90 s, and the sections were washed with phosphate buffered solution (PBS) when the sections were cooled at room temperature. Subsequently, 5% bovine serum albumin (BSA) sealing solution was added and incubated for 30 min at 37 °C. Diluted primary rabbit antibody CAV3 (1:100–1:200, ab2912, Abcam, Inc., MA, USA) was added into sections for incubation at 4 °C overnight. After PBS washing, the sections were added with the diluted secondary goat antibody against rabbit labeled biotin (1:100, HY90046, Shanghai Heng Yuan Biotechnology Co., Ltd., Shanghai, China) for incubation at 37 °C for 30 min. Streptomycin anti-biotin protein-peroxidase solution (Beijing Zhongshan Biotechnology Co., Ltd., Beijing, China) was added for 30-min incubation at 37 °C after an additional round of PBS washing. The sections were then developed by diaminobenzidine (DAB) (Beijing Bioss Biotechnology Co., Ltd., Beijing, China) at room temperature with a final round of PBS washing, immersed in hematoxylin for 5 min and washed under running tap water. Next, the sections were dipped with 1% hydrochloric ethanol for 4 s and turned back to blue for 20 min via tap-water washing. Verification was obtained regarding the positive expression of the CAV3 protein in the event a brown color was observed. Image-Proplus analyzed software (Media Cybernetics, Inc., Rockville, MD, USA) was used to detect the mean optical density (OD) of the positive CAV3 under a high powered lens for quantitative analyses purposes [15].

CAV3 adenovirus expression vector construction

Disposed by RNAi technology, siRNA-CAV3 adenovirus expression vector, NC-siRNA-CAV3 vector, overexpressed adenovirus vector of Ad-CMA-cav-1-eGFP and blank adenovirus vector of Ad-CMV-eGFP were constructed by plasmid pLenR-GFP employed as a vector. The specific siRNA sequence that targeted CAV3 gene was designed to synthesize the double-strand DNA oligo containing interference sequence based on the mRNA sequence of the NCBI nucleotide CAV3, which was directly linked to enzyme digested vector (Engreen Biosystem Co., Ltd., Beijing, China).

Cell culture in vitro and transfection

The parietal bone of the model mice was extracted at the 12th-week post model establishment, and sheared with soft tissue in surface curettage. The samples were detached using 0.25% trypsin at 37 °C with the solution abandoned after 30 min, followed by continual detaching with 0.1% collagenase of I type and selected through a 100-mesh metal sieve. After washing with Hank's solution, the cell concentration of 1×10^5 cells/ml was attained using 10% Dulbecco's modified eagle medium (DMEM). Next, the cells were inoculated into a 48-well plate with a total of 45 wells used and 0.5 ml placed in each one, followed by incubation under saturated humidity conditions at 37 °C with 5% CO_2. The medium was replaced at regular intervals on alternate days. Following that, the medium was replaced on the 3–4 d of passaged osteoblast, and the passage was continued when cell confluency had reached 80%. The 3rd–4th generation osteoblasts were appropriately adopted in the experiment.

The above cultured osteoblasts were divided into six groups: normal group (normal rat osteoblasts without any treatment), normal + si-CVA3 group (normal rat osteoblasts transfected with si-CVA3), control group (osteoporotic rat osteoblasts without any treatment), blank group (osteoporotic rat osteoblasts transfected with blank vector), NC group (osteoporotic rat osteoblasts with transfected with NC vector), si-CAV3 group (osteoporotic rat osteoblasts

Table 1 Primer sequence for RT-qPCR

Gene	Primer sequence (5'-3')
CAV3	Forward: CTGGTCGGTCTACCTCTTCTC
	Reverse: CGACCACGACCACAAACA
β-catenin	Forward: GGAGTTGGACATGGCCATGG
	Reverse: TCCACATCCTCTTCCTCAGG
LRP5	Forward: GATACAGGCACTGACAGAATTG
	Reverse: CCGCTTTGTCCCGTCTAT
TCF	Forward: GTTCACCCACCCGTCCTT
	Reverse: GGCTTCTTCGCCTCCTTCT
Wnt3a	Forward: GTGGTCGCAGCCTGACTT
	Reverse: GCTCTGTGGGCACCTTGA
GAPDH	Forward: CCTGGAGAAACCTGCCAAGTAT
	Reverse: AGCCCAGGATGCCCTTTAGT

RT-qPCR reverse transcription quantitative polymerase chain reaction, *GAPDH* glyceraldehyde-3-phosphate dehydrogenase, *CAV3* caveolin-3, *LRP5* low-density lipoprotein receptor-related protein 5, *TCF* T-cell factor

transfected with siRNA-CAV3), oe-CAV3 group (osteoporotic rat osteoblasts with transfected CAV3 overexpression vector). The osteoblasts were passaged on the day before transfection, and inoculated to a 6-well plate with 1×10^5 cells/well. Cell confluency was confirmed to have reached 70–80% on the day of transfection. The prepared adenovirus particle solution was used to transfect the cells, which were later incubated in a 5% CO_2 incubator at 37 °C, with the medium changed after 6–8 h followed by continued culturing for 24–48 h.

Reverse transcription quantitative polymerase chain reaction (RT-qPCR)

The right-side femur of rats that had the muscle and tendon removed was added with liquid nitrogen and ground to fine powder. Total RNA was extracted using the Trizol (No: 15596-018, Invitrogen Inc., Carlsbad, CA, USA) method for concentration and purity determination purposes. RNA was reversed to cDNA in a total of 25 μl in accordance with the instructions of the Primescript™ RT Reagent kit reverse transcription kit (TaKaRa Engineering Co., Ltd., Liaoning, China). Next, 65 μl of diethylpyrocarbonate (DEPC) water was added to dilute the cDNA and then mixed completely. Fluorescent quantitative PCR was then employed with the cDNA according to the instructions of SYBR® Premix Ex Taq™ II kit (TaKaRa Engineering Co., Ltd., Liaoning, China). The reaction system (50 μl) included 25 μl of SYBR® Premix Ex Taq™ II (2×), 2 μl of PCR upstream primer, 2 μl of PCR downstream primer, 1 μl of ROX Reference Dye (50×), 4 μl of DNA template and 16 μl of dH_2O. Fluorescent quantitative PCR was subsequently performed in the system of ABI PRISM® 7300 (ABI Company, Oyster Bay, NY, USA). The reaction conditions employed were as follows: pre-denaturation at 95 °C for 4 min, 40 cycles of denaturation at 94 °C for 30 s, annealing at 58 °C for 30 s, elongation at 72 °C for 1 min and elongation at 72 °C for 7 min in the last cycle. Glyceraldehyde-3-phosphate dehydrogenase (GAPDH) was considered to be the internal reference with all the primers designed and synthesized by Wuhan Bojie Bioengineering Company (Wuhan Bojie Bioengineering Co., Ltd., Hubei, China) (Table 1). The relationship of multiple proportions of gene expression between experiment group and control group was assessed in accordance with the $2^{-\Delta\Delta Ct}$ and the formulas were as the following: $\Delta\Delta Ct = \Delta Ct_{\text{experiment group}} - \Delta Ct_{\text{control group}}$ and $\Delta Ct = Ct_{\text{target gene}} - Ct_{GAPDH}$. The experiment was repeated 3 times (this assay also appropriate for cell experiment).

Western blot analysis

The right-side femur of rats that had the muscle and tendon removed was added with liquid nitrogen and ground to fine powder. After that, lysate (C0481; Sigma-Aldrich Chemical Company, Ltd., St Louis MO, USA) was added for centrifugation purposes at 13,000 rpm at 4 °C for 15 min, followed by extraction of the supernatant. Protein quantitative analysis was performed by bicinchoninic acid (BCA). A 10% sodium dodecyl sulfate (SDS) separation gel and spacer gel was generated. The sample and the buffer were mixed, boiled at 100 °C for 5 min, ice bathed, centrifuged and added into each lane using a micropipette for electrophoresis purposes. The protein on the gel was then transferred onto a nitrocellulose membrane prior to processing 5% skimmed milk powder at 4 °C and sealing overnight. The primary antibodies CAV3 (1:1000, ab93952), β-catenin (1:5000, ab32572), LRP5 (1: 1000, ab38311), TCF (1:25000, ab76151) and Wnt3a (1:10,000, ab172612, Abcam, Inc., Cambridge, MA, USA) were added for incubation overnight, after which the sample was washed 3 times (5 min for each time) with PBS at room temperature. After the dropwise addition of horse reddish peroxidase (HRP) labeled IgG secondary antibody (1:1000), the membrane was incubated for 1 h at 37 °C, followed by 3 additional PBS washes. Later, the reactive membrane was completely soaked in electrochemiluminescence (ECL) solution (No: 36208ES60, Shanghai Yeasen Biotechnology Co., Ltd., Shanghai, China). Finally, images were acquired in order to evaluate the results by means of exposure in a dark room. With GAPDH as the internal reference, the ratio of grey value between target bands and reference bands was considered to be reflective of the comparative expression of proteins. The experiment was repeated 3 times using 3 samples from each group (this assay also appropriate for cell experiment).

Immunofluorescence double-labeling assay

The well-growing cells were inoculated in a culture dish covered by the 1 cm × 1 cm cover glass with 2×10^4 cells/ml for 1 h. When the cells were confirmed to be fully covered by the glide under a microscope, the culture fluid was removed and the cells were washed twice using 0.01 M PBS and fixed in 4% paraformaldehyde for 30 min. The prepared cell slide was preserved at 20 °C. The cell slides were washed three times PBS (5 min each), sealed with 2% normal goat serum at room temperature for 20 min, incubated with rabbit antibody against CAV3 (1:20, ab2912, Abcam, Inc, MA, USA) and goat antibody against LRP5 (1:50, ab36121, Abcam, Inc, MA, USA) at 37 °C for 1 h followed by PBS shaking and washing. The cells were then incubated with fluorescent-labeled sheep antibody against rabbit IgG (1:100) at 37 °C for 1 h followed by PBS shaking and washing 3 times (5 min each). The cells were added with diamidino-phenyl-indole (DAPI) (ab104139, 1:100, Abcam, Inc, MA, USA) at room temperature for 10 min under conditions void of light, followed by 3 PBS washes (5 min each), sealing and laser scanning confocal microscopy observation.

MTT assay

After transfection, 100 μl of cell suspension was inoculated into a 96-well plate (2×10^3 cells in each well) and incubated in a 5% CO_2 incubator at 37 °C. After a 48 h period of incubation, serum-free medium was added for culture continuation at 37 °C with 5% CO_2. At the 0 h, 24 h, 48 h, and 72 h time points, 20 μl of MTT (5 mg/ml) was added to the wells accordingly. After an additional 4 h period of culturing, the supernatant was discarded. Dimethyl sulfoxide (DMSO) was subsequently added into wells (100 μl/well) and well mixed. After 5 min, microplate reader (Multiskan FC; Thermo Fisher Scientific Inc., NY, USA) was employed to detect OD at a wavelength of 490 nm. The mean was acquired based on the values obtained from ten parallel wells in each group. The above experiment was repeated 3 times and performed by the same individual. A figure of cell viability was drawn with the *x*-axis representing time and the *y*-axis representing OD value. The intra-assay and inter-assay coefficient of variation was less than 5%.

Flow cytometry

After 48 h of transfection, the culture medium was removed, with the cells subsequently washed once with PBS solution. Next, 0.25% trypsin was used to digest the cells until they were confirmed to have assumed a round shape under microscope observation, after which the trypsin was removed. The culture medium containing serum was added to terminate digestion. The cell suspension was obtained after the isolation of cell from cytoderm and then centrifuged at 1000 rpm for 5 min with the supernatant removed accordingly. After two PBS solution washes, the cells were fixed using precooled 70% ethanol for 30 min, centrifuged and collected. After additional PBS washing, the cells were stained with 1% propidium iodide (PI) containing RNA enzyme for 30 min. PI was washed off by means of two PBS washes, with its volume then adjusted to 1 ml by PBS. Finally, cell cycle was calculated by placing the samples into BD-Aria FACS Calibur flow cytometry (FACSCalibur; Beckman Coulter, Inc., Chaska, MN, USA) (3 samples in each group and the experiments were repeated 3 times).

After 48 h of transfection, the cells were detached using trypsin with no ethylenediamine tetraacetic acid (EDTA), collected into a flow tube and centrifuged, after which the supernatant was abandoned. Following 3 PBS washes, the cells were centrifuged with the supernatant abandoned again. As per the instructions of the Annexin-V-fluorescein isothiocyanate (Annexin-V-FITC) cell apoptosis kit (APOAF, Sigma-Aldrich Chemical Company, San Francisco, California, USA) Annexin-V-FITC, PI and hydroxyethyl piperazine ethanesulfonic acid (HEPES) buffer solutions were used to prepare the Annexin-V-FITC/PI staining solution at the ratio of 1:2:50. And then, 1×10^6 cells were resuspended within every 100 μl of staining solution. After mixing, the cells were incubated for 15 min at room temperature, followed by the addition of 1 ml of HEPES and even mixing. The FITC and PI fluorescence was detected at excitation of 525 and 620 nm bandpass filter for cell apoptosis detection purposes. The experiment was repeated 3 times with 3 samples from each group selected in order to calculate the mean value using the following formula: Apoptosis index (AI) = apoptosis cells / (apoptosis cells + normal cells).

Statistical analysis

SPSS 22.0 (IBM Corp. Armonk, NY, USA) statistical analysis software was used for all experimental data processing. Measurement data were expressed as the mean ± standard deviation, and the comparisons between two groups were analyzed using the *t*-test, while one-way analysis of variance was used for comparisons among multiple groups. $p < 0.05$ was considered to be indicative of statistical significance.

Results

Indications of establishing osteoporotic rat models

After 3 weeks of modeling, rats in the osteoporosis group exhibited progressive sluggish activity with sparse hair and

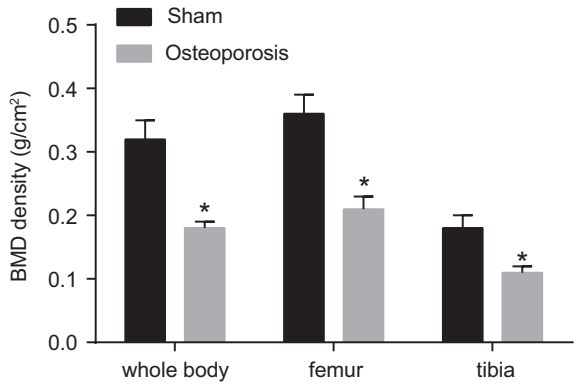

Fig. 1 Significantly decreased bone density was detected in osteoporotic rats. *$p < 0.05$ vs. the sham group. $N = 25$; the data were presented as the mean ± standard deviation, and the comparisons between two groups were analyzed using *t*-test

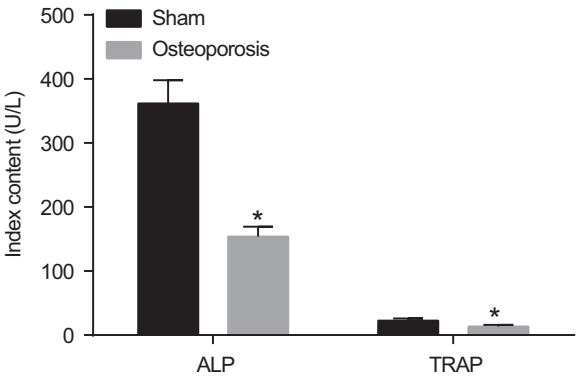

Fig. 3 The serum levels of ALP and TRAP were lower in the osteoporosis group. ALP, alkaline phosphatase; TRAP, tartrate-resistant phosphatase; *$p < 0.05$ vs. the sham group. $N = 25$; the data were presented as the mean ± standard deviation, and the comparisons between two groups were analyzed using *t*-test

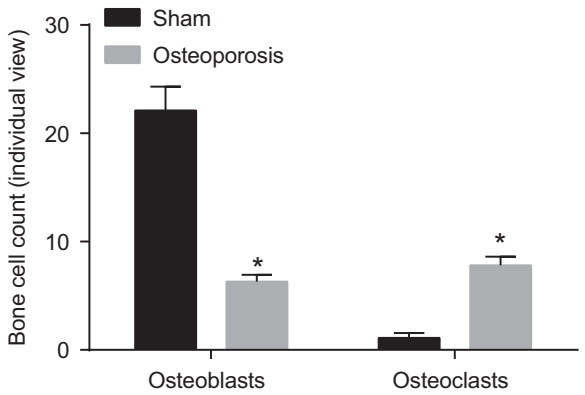

Fig. 2 Decreased osteoblasts while increased osteoclasts were observed in the osteoporosis group. *$p < 0.05$ vs. the sham group. $N = 4$; the data were presented as the mean ± standard deviation, and the comparisons between two groups were analyzed using *t*-test

drooping spirit. In contrast, the sham group was observed to have thick hair and normal activity and spirit. After 12 weeks of modeling, bone density (including whole-body bone, femur, and tibia) of osteoporotic rats markedly decreased compared with the sham group. Based on the aforementioned observations we concluded that the osteoporotic rat model had been successfully established (Fig. 1).

Osteoporotic rats exhibit decreased numbers of osteoblast and increased osteoclast

The number of osteoblasts in the cancellous bone area at metaphysis distal to left-side femurs detected was as follows: the sham group (22.11 ± 2.21), the osteoporosis group (6.31 ± 0.63). And the number of osteoclasts in the cancellous bone area at metaphysis distal to left-side femurs was: the sham group (1.11 ± 0.49), the osteoporosis group (7.81 ± 0.81). The obtained results indicated that the number of osteoblasts was reduced while that of the osteoclasts was increased in the osteoporosis group when compared with sham-operated rats ($p < 0.05$) (Fig. 2).

Osteoporotic rats display decreased serum ALP and TRAP levels

In the sham group, serum ALP and TRAP levels were respectively (361.89 ± 36.18) U/L and (22.56 ± 3.35) U/L. In the osteoporosis group, serum ALP and TRAP levels were confirmed to have reached (153.84 ± 15.38) U/L and (13.71 ± 2.22) respectively, highlighting decreased serum ALP and TRAP levels in the osteoporosis group compared with the sham group ($p < 0.05$) (Fig. 3).

Pathological changes in rat bone tissues

In an attempt to further ascertain as to whether the rat model of osteoporosis had been successfully established, the bone tissues of the rats were analyzed. In the sham group, the bone trabecula of the femur was thick and large, with a compact structure and scarce bone lacuna, in addition to widening of the cartilage of the femur epiphyseal plate and a large number of cartilage cells (Fig. 4a). In relation to the osteoporosis group, reduced, thinner, and even fractured bone trabecula was observed, in addition to a greater distance among bone trabecula. Besides, a narrower cartilage of the femur epiphyseal plate was presented and the number of cartilages decreased with a dissolved columnar arrangement (Fig. 4b).

Modeled rats exhibit a lower positive expression rate of CAV3

Immunochemistry methods were performed to detect the positive expression of CAV3 in bone tissues of the modeled

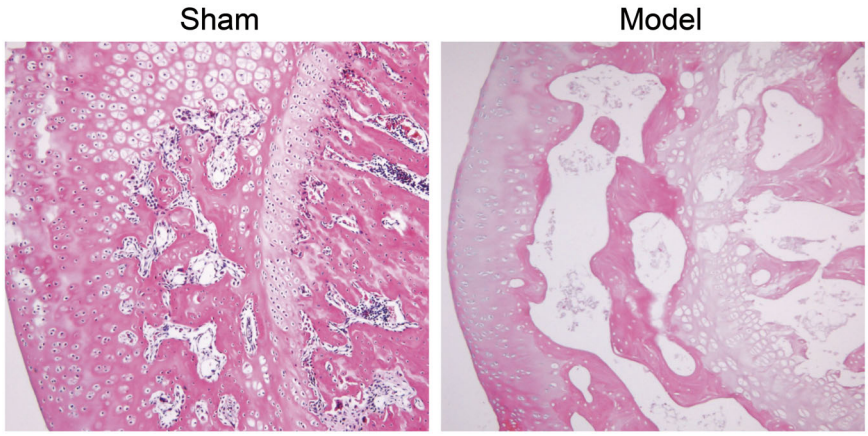

Fig. 4 Pathologic changes of bone tissues detected by HE staining in the sham and osteoporosis groups (× 400). HE, hematoxylin-eosin

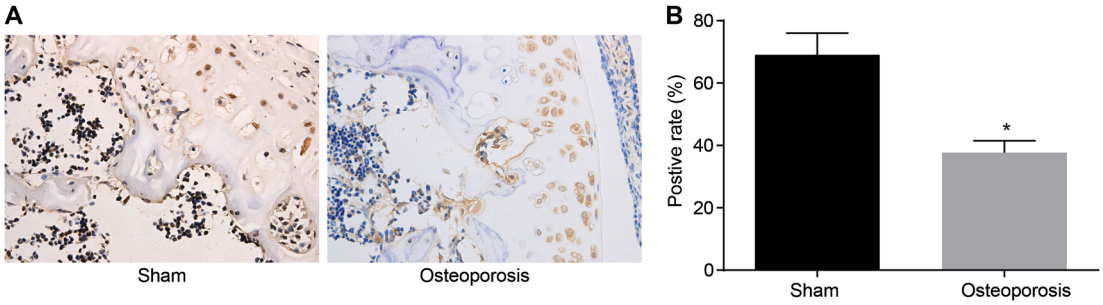

Fig. 5 Lower positive expression rate of CAV3 was found in the osteoporosis group. **a** immunohistochemical map of CAV3 (× 400); **b** the positive expression rate of CAV3 protein; *$p < 0.05$ vs. the sham group. $N = 6$; the data were presented as the mean ± standard deviation, and the comparisons between two groups were analyzed using *t*-test

rats, the results of which revealed that the positive expression rate of CAV3 protein was 69.08% ± 6.92% in the sham group, while 37.69% ± 3.79% in the osteoporosis group. The results obtained indicated there to be a lower positive expression rate of CAV3 protein in the osteoporosis group when compared with the sham group (Fig. 5a, b).

Cell transfection effectiveness

After cell transfection, no green fluorescence expression was detected in the normal and control groups when analyzed under a fluorescence microscope, while the amount of green fluorescence expression was detected in the normal + si-CAV3, blank, NC, si-CAV3 and oe-CAV3 groups (over 80% expression rate was achieved). There was no significant difference observed in relation to the transfection efficacy of the normal + si-CAV3, blank, NC, si-CAV3 and oe-CAV3 groups ($p > 0.05$). The aforementioned findings suggested that the vectors of siRNA-CAV3, NC-siRNA-CAV3, Ad-CMV-cav-3-eGFP, and Ad-CMV-eGFP had indeed been successfully transfected into the bone cells which was accompanied by efficacy expression (Fig. 6a–c).

si-CAV3 in osteoporotic rats decreases the mRNA and protein expression of CAV3, β-catenin, LRP5, TCF, and Wnt3a

The mRNA and protein expression of CAV3, β-catenin, LRP5, TCF, and Wnt3a among the osteoblasts was detected by means of RT-qPCR and western blot analysis. Compared with the normal group, lower levels of mRNA and protein expressions of CAV3, β-catenin, LRP5, TCF, and Wnt3a were detected in the normal + si-CAV3, control, blank, NC and si-CAV3 and oe-CAV3 groups. The mRNA and protein expression of CAV3, β-catenin, LRP5, TCF, and Wnt3a exhibited markedly decreased levels in the si-CAV3 group when compared with the control group, while a distinct increase in terms of the mRNA and protein expression of CAV3, β-catenin, LRP5, TCF, and Wnt3a was detected in the oe-CAV3 group (all $p < 0.05$). No significant difference was observed between the control group and the blank and NC groups ($p > 0.05$) (Fig. 7a–c). Immunofluorescence double-labeling assay demonstrated that CAV3 and LRP5 were co-localized in the cell membrane (Fig. 7d). The above results suggested that overexpressed CAV3 could activate the Wnt signaling pathway in the presence of osteoporosis.

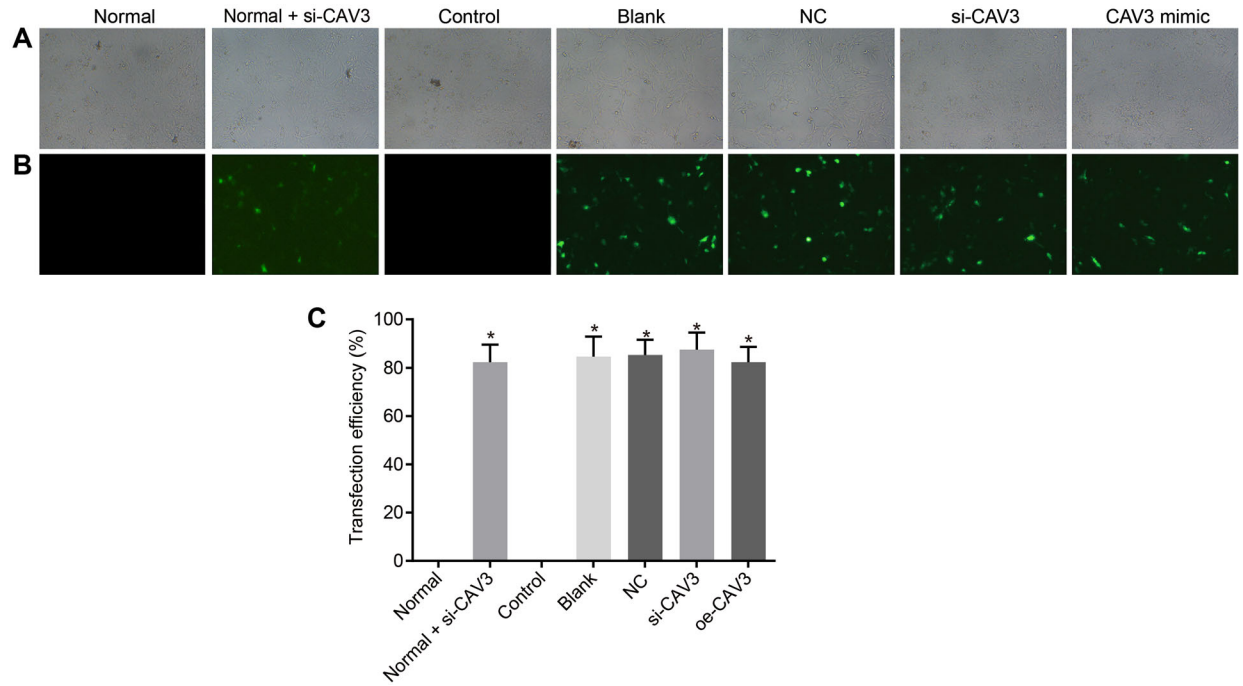

Fig. 6 Successful transfection of adenovirus vector into bone tissues (× 100). **a** Bright field of cells in six groups; **b** fluorography of cells in six groups; **c** the cell transfection efficacy in each group. *$p < 0.05$ vs. the normal and blank groups. Measurement data were expressed as the mean ± standard deviation, one-way analysis of variance was used for comparisons among multiple groups. The experiment was conducted independently 3 times

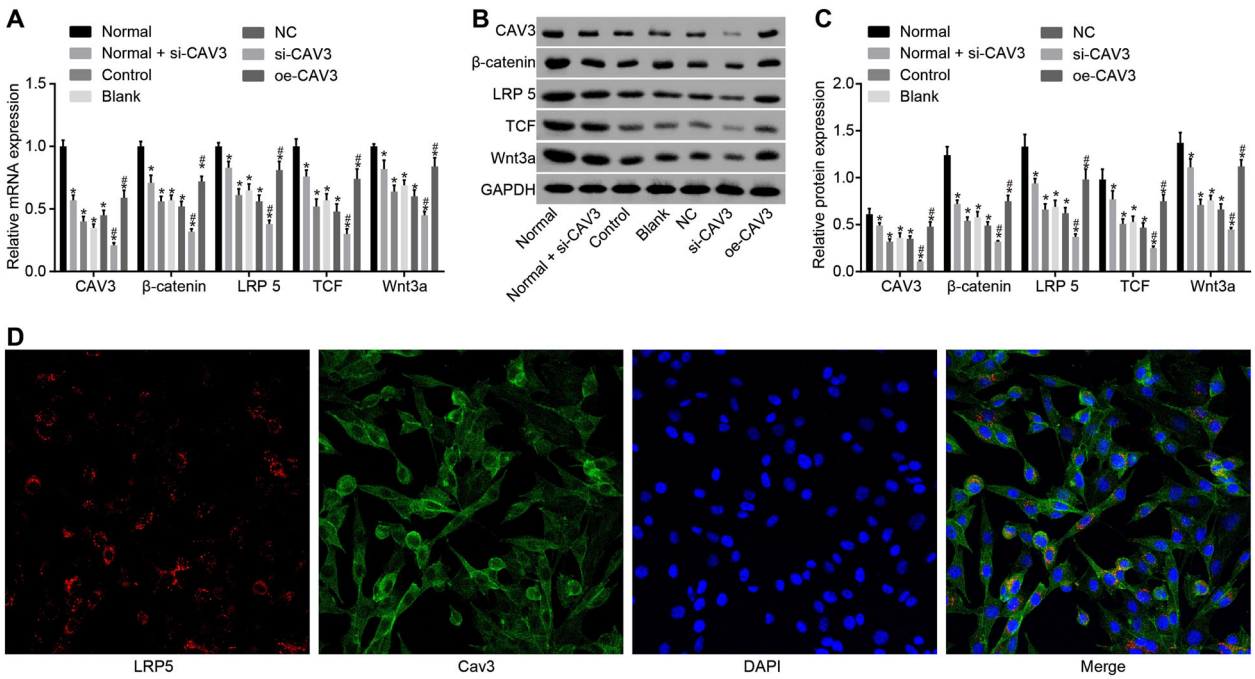

Fig. 7 Overexpression of CAV3 increased the expression of β-catenin, LRP5, TCF, and Wnt3a. **a** mRNA expression of CAV3, β-catenin, LRP5, TCF, and Wnt3a; **b** protein expression of CAV3, β-catenin, LRP5, TCF, and Wnt3a; **c** western blot analysis of CAV3, β-catenin, LRP5, TCF, and Wnt3a; CAV3, caveolin-3; **d** immunofluorescence double-labeling detection of CAV3 and LRP5 (× 400). Measurement data were expressed as the mean ± standard deviation, one-way analysis of variance was used for comparisons among multiple groups. The experiment was conducted independently 3 times.LRP-5, low-density lipoprotein receptor-related protein-5; TCF, T cell factor; *$p <$ 0.05 vs. the normal group; $^{\#}p < 0.05$ vs. the control group

CAV3 silencing inhibits cell proliferation

In order to determine the effect of CAV3 on the osteoblast proliferation in osteoporosis, MTT assay was employed to determine cell viability, the results of which indicated there to be no significant differences at 0 h. Compared with the normal group, cell viability exhibited slowed rates in the groups at 24 h, 48 h, and 72 h ($p < 0.05$). Compared with the control group, decreased cell viability was detected in the si-CAV3 group while an opposite trend was observed in the oe-CAV3 group ($p < 0.05$). There was no obvious difference between the control group and the blank and NC groups ($p > 0.05$). The above results suggested overexpressed CAV3 promoted osteoblast proliferation markedly (Fig. 8).

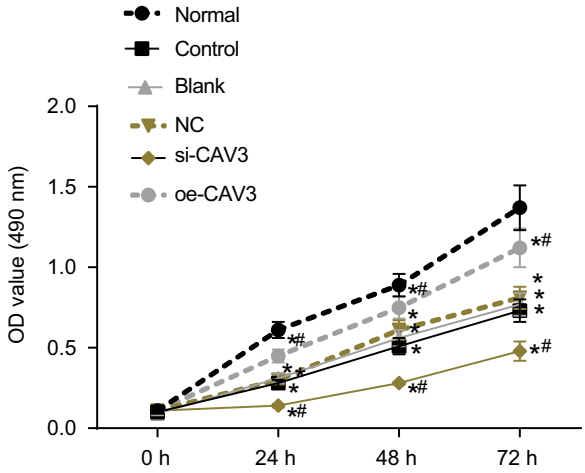

Fig. 8 The MTT assay revealed that cell proliferation at the point of 0 h, 24 h, 48 h, and 72 h was inhibited after transfected with si-CAV3. Measurement data were expressed as the mean ± standard deviation, repetitive analysis of variance was used for comparisons among multiple groups. The experiment was conducted independently 3 times.*$p < 0.05$ vs. the normal group; #$p < 0.05$ vs. the control group

CAV3 silencing arrests cells at the G1 phase

PI single staining was applied in order to detect the effect of CAV3 on osteoblast cycle in osteoporosis. In comparison with the normal group, the rat bone cell ratio was elevated at the G1 phase while diminished numbers were detected at the S phase in all the other groups ($p < 0.05$). Compared with the control group, higher cell ratio at the G1 phase and a smaller cell ratio at the S phase were observed in the si-CAV3 group while contrasting trends were observed in the oe-CAV3 group ($p < 0.05$). No significant differences between the control blank and NC groups were detected ($p > 0.05$) (Fig. 9a, b). Overexpressed CAV3 was subsequently confirmed to arrest osteoblasts at the S phase in osteoporosis.

CAV3 silencing increased cell apoptosis

Annexin V-FITC/PI staining was employed to determine the effect of CAV3 on osteoblast apoptosis in osteoporosis.

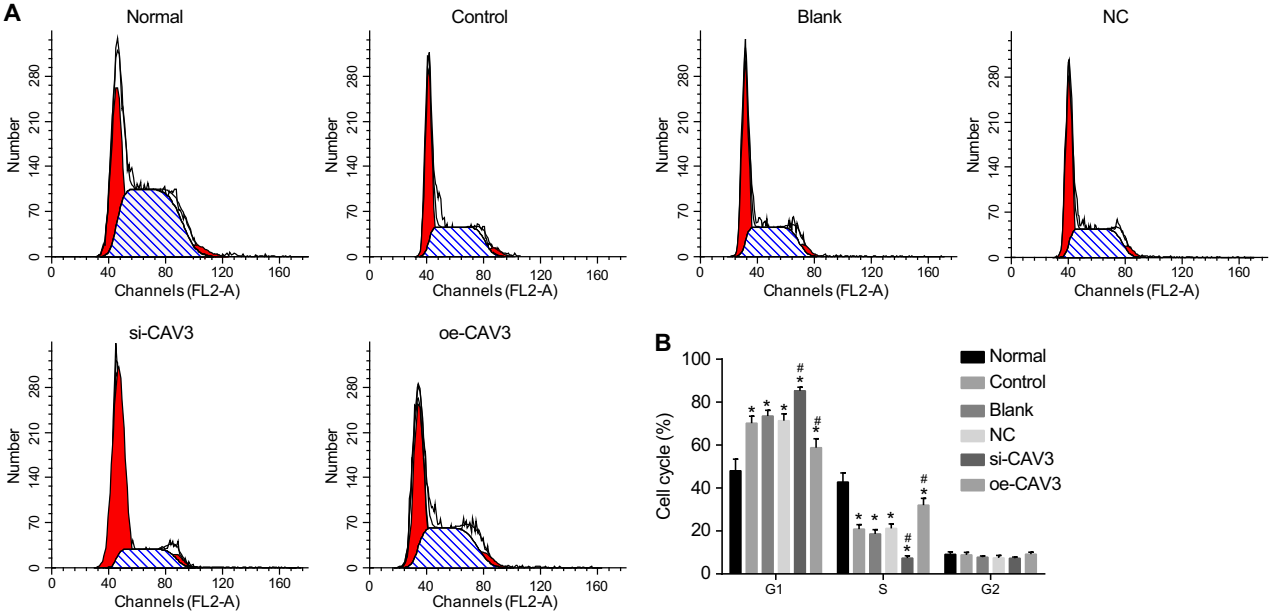

Fig. 9 Cells were arrested in G1 phase after transfected with si-CAV3. **a** cell cycle distribution in six groups; **b** cell cycle ratio in six groups; *$p < 0.05$ vs. the normal group; #$p < 0.05$ vs. the control group. Measurement data were expressed as the mean ± standard deviation, one-way analysis of variance was used for comparisons among multiple groups. The experiment was conducted independently 3 times

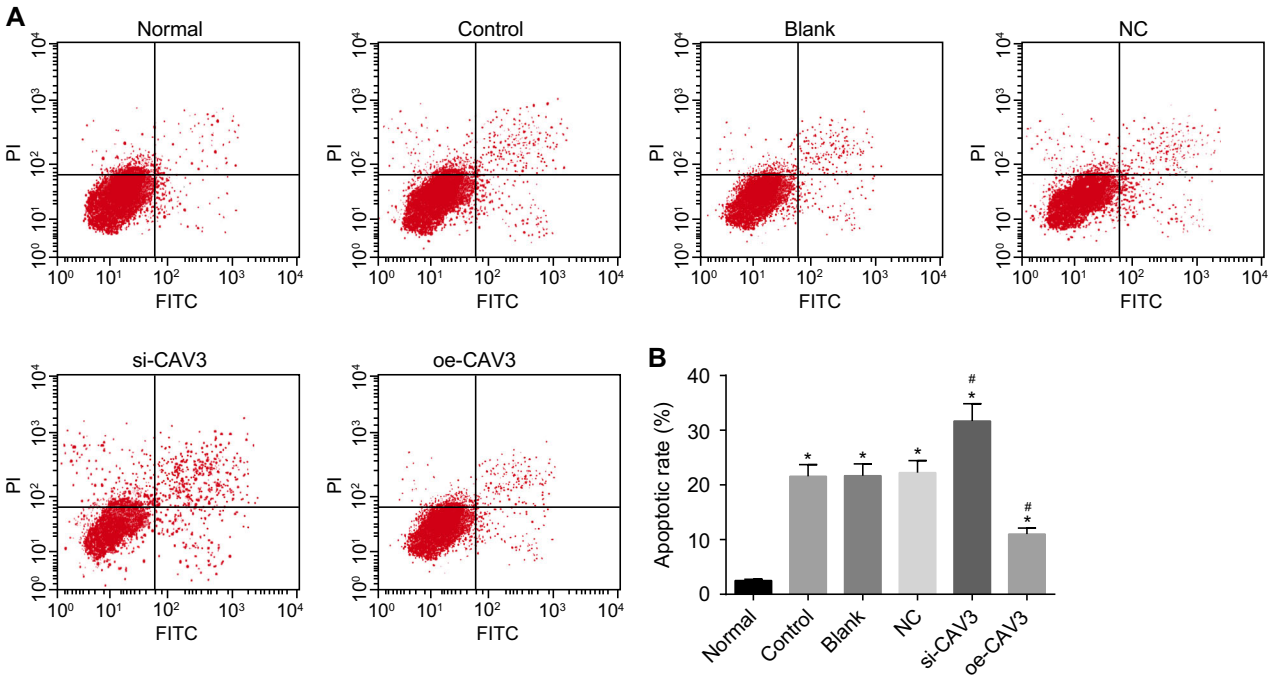

Fig. 10 Annexin V-FITC/PI double standard staining demonstrated that cell apoptosis was promoted following the transfection of si-CAV3. **a** cell apoptosis profile in six groups; **b** histogram of apoptosis in six groups; $^{*}p < 0.05$ vs. the normal group; $^{\#}p < 0.05$ vs. the control group. Measurement data were expressed as the mean ± standard deviation, one-way analysis of variance was used for comparisons among multiple groups. The experiment was conducted independently 3 times

Compared with the normal group, increased cell apoptosis was detected in the other groups ($p < 0.05$). No significant difference was found between the control group and the blank and NC groups. Compared with the control group, increased cell apoptosis was detected in the si-CAV3 group while a reduced rate of apoptosis was observed in the oe-CAV3 group ($p < 0.05$) (Fig. 10a, b). Overexpressed CAV3 may inhibit osteoblast apoptosis in osteoporosis.

Discussion

Osteoporosis continues to plague millions of individuals worldwide on an annual basis. The condition is characterized by an impairment of bone mass that results in declined bone formation and a higher incidence of fragility fractures, significantly threatening the quality of life particularly among the aging population. Deeper investigations into the reaction involving bone biology, molecular mechanism, and signaling network may well provide greater insight and greater identification of novel therapies [16]. During the current study, the central objective was to elucidate the mechanism by which the silencing of CAV3 influences bone formation and osteoporosis precession via the Wnt signaling pathway in an ovariectomized rat model of osteoporosis, in order to identify the possible role of CAV3 in human cellular and molecular microenvironment of osteoporosis.

As indicated by our results, the osteoporotic rats displayed decreased levels of ALP, TRAP as well as mRNA and positive expressions of CAV3. It is widely accepted throughout the literature that sufficient osteoblasts cells are critical to bone formation, namely, deficient osteoblasts lead to bone loss, a process which is exaggerated among individuals troubled with osteoporosis [17]. In addition. accelerated osteoclast cell growth was confirmed to be a key trigger inducing osteoporosis [18]. As one noncollagenous protein secreted by osteoblast, ALP is essential for bone mineralization [19]. Increased ALP expression has been linked to conditions like rapid bone loss and increased risk of bone fracture [20]. TRAP is highly expressed in osteoclasts and reported to be involved in osteoclast-mediated bone turnover [21]. CAV3 is expressed predominantly in muscle tissue types, including skeletal muscle, diaphragm, and heart, and is selectively induced during the differentiation of skeletal C2C12 myoblasts [22]. The aforementioned findings provided elucidation to the intricate crosstalk between related genes and osteoporosis, laying a good foundation for a further study on microenvironment around osteoporosis progression.

Silencing of CAV3 resulted in reduced levels of β-catenin, LRP5, TCF, and Wnt3a in the osteoporotic rat

osteoblasts, which means that CAV3 is able to activate the Wnt signaling pathway. Correspondingly, evidence has been presented in the literature indicating that silenced CAV1, which is a family member of CVA3, could reduce β-catenin pathway from a mechanistic and clinical investigation perspective [23]. CAV3 has been reported to downregulate the activity of the Wnt signaling pathway and has been implicated as a key factor behind the reduced bone formation. LRP5, is a type of Wnt signaling pathway component that is impaired in osteoporosis [24, 25]. What's more, Wnt3a has been suggested to share a positive correlation with Wnt/β-catenin signaling as it was an activator of the Wnt/β-catenin signaling pathway [26]. In addition, it has been revealed that the deleted β-catenin significantly influences the reduction of bone formation [27]. Convicted evidence suggests that mutant components of the β-catenin complex or included in the β-catenin gene account for the functional performance of β-catenin and Wnt/β-catenin pathway [28], which essentially suggests there to be a similar trend between Wnt and β-catenin. Investigation into the Wnt proteins during our study revealed that it is closely related to LRP5, one of its cell surface receptors [29]. Besides, TCF signaling was a promotor to the bone formation [30], thus the loss of TCF had the positive effects on osteoporosis. What's more, β-catenin has been shown to play a key role through Wnt-mediated regulation in the presence of the cytoplasm, interacting with the TCF of transcription factors to stimulate downstream gene expression [31] ultimately suggesting that the loss of CAV3 downregulates Wnt signaling and the factors activating in it, straightening out the relations of these cell factors.

Finally, downregulated CAV3 could inhibit bone cell proliferation and accelerate the apoptosis of the osteoporotic rats via regulating positively the Wnt signaling pathway. Caveolin-1 and CVA3 could act as scaffolding proteins that negatively mediate the activity or the release of many molecules, including pro-proliferative, oncogenic, and antiapoptotic proteins [32]. From another perspective, Wnt1-inducible signaling protein-3 (WISP3) silencing has been demonstrated to reduce gastric cancer cell proliferation by weakening β-catenin activity and suppressing Wnt/β-catenin pathway and its target gene in downstream, similar to LRP5, and TCF which we previously mentioned [33]. The activity of Wnt signaling has been indicated in recent literature to affect the processes of apoptosis, either by accelerating or inhibiting it in relation to specific cellular conditions [34]. Furthermore, our study highlighted the key role played by caveolin in the activation of the Wnt/β-catenin pathway [35].

At present, the function of CAV3 has rarely been investigated, Our study, to a certain degree, highlights a novel perspective in relation to this sorely underexplored field, indicating that CAV3 can accelerate bone formation which results in a reduction in the incidence of osteoporosis via the activation of the Wnt signaling pathway. Based on the key findings of our study, we concluded that the inhibitors of CAV3 have the potential to be developed for the future treatment of osteoporosis.

Acknowledgements We would like to acknowledge the helpful comments on this paper received from our reviewers.

Funding This study was supported by Fuzhou Science and Technology Bureau (No. 2013-S-123-4) and Natural Science Foundation of Fujian Province (No. 2016J01598).

Compliance with ethical standards

Conflict of interest The authors declare that they have no conflict of interest.

Ethical approval All animal operations in this study were performed was in line with the local principles of management and use of experimental animals.

References

1. E.M. Curtis, R.J. Moon, N.C. Harvey, C. Cooper, The impact of fragility fracture and approaches to osteoporosis risk assessment worldwide. Bone **104**, 29–38 (2017)
2. R. Baron, M. Kneissel, WNT signaling in bone homeostasis and disease: from human mutations to treatments. Nat. Med. **19**(2), 179–192 (2013)
3. S.W. Wade, C. Strader, L.A. Fitzpatrick, M.S. Anthony, C.D. O'Malley, Estimating prevalence of osteoporosis: examples from industrialized countries. Arch. Osteoporos. **9**, 182 (2014)
4. N.D. Zhang, T. Han, B.K. Huang, K. Rahman, Y.P. Jiang, H.T. Xu, L.P. Qin, H.L. Xin, Q.Y. Zhang, Y.M. Li, Traditional Chinese medicine formulas for the treatment of osteoporosis: Implication for antiosteoporotic drug discovery. J. Ethnopharmacol. **189**, 61–80 (2016)
5. K. Lippuner, The future of osteoporosis treatment - a research update. Swiss Med. Wkly **142**, w13624 (2012)
6. R. Yuan, S. Ma, X. Zhu, J. Li, Y. Liang, T. Liu, Y. Zhu, B. Zhang, S. Tan, H. Guo, S. Guan, P. Ao, G. Zhou, Core level regulatory network of osteoblast as molecular mechanism for osteoporosis and treatment. Oncotarget **7**(4), 3692–3701 (2016)
7. J. Cheng, C.R. Valdivia, R. Vaidyanathan, R.C. Balijepalli, M.J. Ackerman, J.C. Makielski, Caveolin-3 suppresses late sodium current by inhibiting nNOS-dependent S-nitrosylation of SCN5A. J. Mol. Cell. Cardiol. **61**, 102–110 (2013)
8. P. Nassoy, C. Lamaze, Stressing caveolae new role in cell mechanics. Trends Cell Biol. **22**(7), 381–389 (2012)
9. M. Maceckova, H. Martiskova, A. Koudelka, L. Kubala, A. Lojek, M. Pekarova, Bone marrow-derived macrophages exclusively expressed caveolin-2: the role of inflammatory activators and hypoxia. Immunobiology **220**(11), 1266–1274 (2015)
10. C. Niehrs, The complex world of WNT receptor signalling. Nat. Rev. Mol. Cell Biol. **13**(12), 767–779 (2012)
11. J.N. Anastas, R.T. Moon, WNT signalling pathways as therapeutic targets in cancer. Nat. Rev. Cancer **13**(1), 11–26 (2013)
12. D.G. Monroe, M.E. McGee-Lawrence, M.J. Oursler, J.J. Westendorf, Update on Wnt signaling in bone cell biology and bone disease. Gene **492**(1), 1–18 (2012)

13. G. Yuan, I. Regel, F. Lian, T. Friedrich, I. Hitkova, R.D. Hofheinz, P. Strobel, R. Langer, G. Keller, C. Rocken, W. Zimmermann, R.M. Schmid, M.P. Ebert, E. Burgermeister, WNT6 is a novel target gene of caveolin-1 promoting chemoresistance to epirubicin in human gastric cancer cells. Oncogene **32**(3), 375–387 (2013)
14. H. Namkung-Matthai, R. Appleyard, J. Jansen, J. Hao Lin, S. Maastricht, M. Swain, R.S. Mason, G.A. Murrell, A.D. Diwan, T. Diamond, Osteoporosis influences the early period of fracture healing in a rat osteoporotic model. Bone **28**(1), 80–86 (2001)
15. K. Jensen, R. Krusenstjerna-Hafstrom, J. Lohse, K.H. Petersen, H. Derand, A novel quantitative immunohistochemistry method for precise protein measurements directly in formalin-fixed, paraffin-embedded specimens: analytical performance measuring HER2. Mod. Pathol. **30**(2), 180–193 (2017)
16. T.D. Rachner, S. Khosla, L.C. Hofbauer, Osteoporosis: now and the future. Lancet **377**(9773), 1276–1287 (2011)
17. P.J. Marie, M. Kassem, Osteoblasts in osteoporosis: past, emerging, and future anabolic targets. Eur. J. Endocrinol. **165**(1), 1–10 (2011)
18. Y. Miyauchi, Y. Sato, T. Kobayashi, S. Yoshida, T. Mori, H. Kanagawa, E. Katsuyama, A. Fujie, W. Hao, K. Miyamoto, T. Tando, H. Morioka, M. Matsumoto, P. Chambon, R.S. Johnson, S. Kato, Y. Toyama, T. Miyamoto, HIF1alpha is required for osteoclast activation by estrogen deficiency in postmenopausal osteoporosis. Proc. Natl. Acad. Sci. USA **110**(41), 16568–16573 (2013)
19. L.M. Havill, L.G. Hale, D.E. Newman, S.M. Witte, M.C. Mahaney, Bone, ALP and OC reference standards in adult baboons (Papio hamadryas) by sex and age. J. Med. Primatol. **35**(2), 97–105 (2006)
20. C. Li, Z. Jiang, X. Liu, Biochemical mechanism of gallium on prevention of fatal cage-layer osteoporosis. Biol. Trace Elem. Res. **134**(2), 195–202 (2010)
21. S. Zenger, K. Hollberg, J. Ljusberg, M. Norgard, B. Ek-Rylander, R. Kiviranta, G. Andersson, Proteolytic processing and polarized secretion of tartrate-resistant acid phosphatase is altered in a subpopulation of metaphyseal osteoclasts in cathepsin K-deficient mice. Bone **41**(5), 820–832 (2007)
22. Z. Tang, P.E. Scherer, T. Okamoto, K. Song, C. Chu, D.S. Kohtz, I. Nishimoto, H.F. Lodish, M.P. Lisanti, Molecular cloning of caveolin-3, a novel member of the caveolin gene family expressed predominantly in muscle. J. Biol. Chem. **271**(4), 2255–2261 (1996)
23. Z. Wang, N. Wang, W. Li, P. Liu, Q. Chen, H. Situ, S. Zhong, L. Guo, Y. Lin, J. Shen, J. Chen, Caveolin-1 mediates chemoresistance in breast cancer stem cells via beta-catenin/ABCG2 signaling pathway. Carcinogenesis **35**(10), 2346–2356 (2014)
24. J. Korvala, H. Juppner, O. Makitie, E. Sochett, D. Schnabel, S. Mora, C.F. Bartels, M.L. Warman, D. Deraska, W.G. Cole, H. Hartikka, L. Ala-Kokko, M. Mannikko, Mutations in LRP5 cause primary osteoporosis without features of OI by reducing Wnt signaling activity. Bmc. Med. Genet. **13**, 26 (2012)
25. M. Rossini, D. Gatti, S. Adami, Involvement of WNT/beta-catenin signaling in the treatment of osteoporosis. Calcif. Tissue Int. **93** (2), 121–132 (2013)
26. R.K. Bikkavilli, C.C. Malbon, Arginine methylation of G3BP1 in response to Wnt3a regulates beta-catenin mRNA. J. Cell. Sci. **124** (Pt 13), 2310–2320 (2011)
27. J. Chen, F. Long, beta-catenin promotes bone formation and suppresses bone resorption in postnatal growing mice. J. Bone Miner. Res. **28**(5), 1160–1169 (2013)
28. J. Su, A. Zhang, Z. Shi, F. Ma, P. Pu, T. Wang, J. Zhang, C. Kang, Q. Zhang, MicroRNA-200a suppresses the Wnt/beta-catenin signaling pathway by interacting with beta-catenin. Int. J. Oncol. **40** (4), 1162–1170 (2012)
29. Z. von Marschall, L.W. Fisher, Secreted Frizzled-related protein-2 (sFRP2) augments canonical Wnt3a-induced signaling. Biochem. Biophys. Res. Commun. **400**(3), 299–304 (2010)
30. S. Iyer, E. Ambrogini, S.M. Bartell, L. Han, P.K. Roberson, R. de Cabo, R.L. Jilka, R.S. Weinstein, C.A. O'Brien, S.C. Manolagas, M. Almeida, FOXOs attenuate bone formation by suppressing Wnt signaling. J. Clin. Invest. **123**(8), 3409–3419 (2013)
31. J. Wang, J.S. Park, Y. Wei, M. Rajurkar, J.L. Cotton, Q. Fan, B.C. Lewis, H. Ji, J. Mao, TRIB2 acts downstream of Wnt/TCF in liver cancer cells to regulate YAP and C/EBPalpha function. Mol. Cell **51**(2), 211–225 (2013)
32. S. Bousserouel, M. Raymondjean, A. Brouillet, G. Bereziat, M. Andreani, Modulation of cyclin D1 and early growth response factor-1 gene expression in interleukin-1beta-treated rat smooth muscle cells by n-6 and n-3 polyunsaturated fatty acids. Eur. J. Biochem. **271**(22), 4462–4473 (2004)
33. F. Fang, W.Y. Zhao, R.K. Li, X.M. Yang, J. Li, J.P. Ao, S.H. Jiang, F.Z. Kong, L. Tu, C. Zhuang, W.X. Qin, P. He, W.M. Zhang, H. Cao, Z.G. Zhang, Silencing of WISP3 suppresses gastric cancer cell proliferation and metastasis and inhibits Wnt/beta-catenin signaling. Int. J. Clin. Exp. Pathol. **7**(10), 6447–6461 (2014)
34. N. Pecina-Slaus, Wnt signal transduction pathway and apoptosis: a review. Cancer Cell. Int. **10**, 22 (2010)
35. H. Yamamoto, H. Komekado, A. Kikuchi, Caveolin is necessary for Wnt-3a-dependent internalization of LRP6 and accumulation of beta-catenin. Dev. Cell. **11**(2), 213–223 (2006)